

Phase-Change Based Interlayer Exchange Coupling Control

Xiaofei Fan,^{1,†} Guodong Wei,^{1,†} Xiaoyang Lin,^{1,2,†,*} Xinhe Wang,¹
Zhizhong Si,¹ Xueying Zhang,^{1,2} Qiming Shao,³ Stephane Mangin,⁴ Eric
Fullerton,⁵ Lei Jiang,⁶ Weisheng Zhao^{1,2,*}

¹ Fert Beijing Research Institute, School of Microelectronics & Beijing Advanced
Innovation Center for Big Data and Brain Computing (BDBC), Beihang University,
Beijing 100191, China

² Beihang-Goertek Joint Microelectronics Institute, Qingdao Research Institute,
Beihang University, Qingdao 266000, China

³ Department of Electronic and Computer Engineering, The Hong Kong University of
Science and Technology, Clear Water Bay, Kowloon, Hong Kong SAR, China

⁴ Institut Jean Lamour, UMR 7198, CNRS-Universite de Lorraine, F-54000 Nancy,
France

⁵ Center for Memory and Recording Research, University of California San Diego,
9500 Gilman Drive, La Jolla, CA 92093-0401, USA

⁶ School of Chemistry, Beihang University, Beijing 100191, China

†These authors contributed equally.

*E-mail: XYLin@buaa.edu.cn (X.Y.L), weisheng.zhao@buaa.edu.cn (W.S.Z)

Abstract

Changing the interlayer exchange coupling between magnetic layers in situ is a key issue for spintronic, as it allows for optimization of properties that are desirable for applications including magnetic sensing and memory. In this paper, we utilize the phase-change material VO₂ as the spacer layer to regulate the interlayer exchange coupling between the ferromagnetic layers with perpendicular magnetic anisotropy. Successful growth of ultra-thin (several nanometers) VO₂ films with metal-to-insulator transition features is realized by sputtering at room temperature, which further enables the fabrication of [Pt/Co]₂/VO₂/[Co/Pt]₂ systems with distinct interfaces. Such a magnetic multilayer system demonstrates an evolution from weak antiferromagnetic coupling to ferromagnetic coupling as the VO₂ undergoes a phase-change. The underlying mechanism originates from the electronic structure change of the spacer layer from insulation to metallicity. As a demonstration of phase-change spintronics, this work may reveal the great potential of materials innovation for next-generation spintronics.

Keywords : phase-change; interlayer exchange coupling; VO₂; spintronics

Introduction

Interlayer exchange coupling (IEC) is an indirect exchange interaction between magnetic layers mediated by the conduction electrons of the spacer layer. The discovery of IEC has given birth to the booming research in spintronics including giant magnetoresistance (GMR)^{1,2} and tunneling magnetoresistance (TMR) effects^{3,4}, and has been extensively applied to the design of synthetic antiferromagnet (SAF) layers in magnetic tunnel junctions (MTJ). Comparing with direct manipulations of magnetizations in spintronic devices, transitions of IEC between ferromagnetic (FM) and antiferromagnetic (AFM) coupling states may provide a promising opportunity to realize low-power spintronic device applications in the post-Moore's-law era⁵⁻⁷. Up to now, IEC has been systematically investigated in layered structures with different metallic spacer layers⁸⁻¹¹, as well as some semiconducting, insulating, and organic spacers, *e.g.*, Si¹²⁻¹⁴, GaAs^{15,16}, MgO^{17,18} and α -sexithiophene¹⁹. The periodically oscillated IEC strength with the thickness variation of metallic spacer layer^{8-10,20} has attracted a great deal of research interest in its physical mechanism. One of the most important theories is the Rudermann–Kittel–Kasuya–Yosida (RKKY) interaction²¹⁻²³, which attributes the magnetic coupling to interactions between localized d- or f-shell electron spins through the conduction electrons. Another commonly accepted theory is based on the quantum well states (QWSs), which describes the discrete electronic states formed by electron confinement, and evolves periodically with the well width²⁴⁻²⁶. Pioneering theoretical researchers have also tried to develop a unified theory for both metallic and insulating spacer layers, by introducing the concept of a complex Fermi surface^{27,28}, although further research is still needed to promote relevant developments.

In most experimental cases, the regulation of IEC is achieved through thickness changing of spacer layer^{29,30}, or external engineering by stress and electrochemistry³¹. However, these methods are usually non-dynamic or even irreversible, which limits the application of IEC in innovative spintronic devices. One possible attempt to solve this problem is to substitute the traditional spacer layer with materials sensitive to external stimuli, utilizing their electronic property change to manipulate IEC directly³²⁻³⁴. From this point of view, phase-change material, such as VO₂, can be a promising candidate

for the spacer layer, benefiting from its feature of near room temperature metal-to-insulator transition (MIT)^{35,36}. In fact, with characteristics of fast-response and high-stability, VO₂ has been extensively studied in the phase-change electronics^{37–39}. Therefore, a VO₂ phase-change based spintronic device may reform the magnetism modulation strategy and enable emerging phase-change spintronic device applications.

In this work, we successfully deposited ultra-thin (several nanometers) VO₂ films using magnetron sputtering at high vacuum, verified by X-ray diffraction (XRD) and X-ray photoelectron spectroscopy (XPS). Phase-change feature of such an ultra-thin film is further proved by electrical transport measurements. [Pt/Co]₂/VO₂/[Co/Pt]₂ multilayer system with perpendicular magnetic anisotropy (PMA) feature is prepared to explore the phase-change induced IEC regulation. By characterizations at different temperatures, the switching from weak antiferromagnetic coupling to ferromagnetic coupling has been observed. The VO₂ thickness dependent switching process has been evaluated and explained by the effect of MIT induced Fermi surface modulations. This work, combining MIT with IEC modulation, shows a fairly groundbreaking and promising approach to take joint advantages of phase-change electronics and spintronics.

Results

Characterization of ultra-thin VO₂ film and preparation of phase-change magnetic multilayer system

For the experiment of phase-change induced IEC regulation, the preparation of VO₂ films with nanometer thickness lies in the heart of all problems. Even though lots of methods have been used to deposit VO₂, such as molecular beam epitaxy⁴⁰, pulsed laser deposition^{41–43} and chemical vapor deposition⁴⁴, strict growth requirements, *e.g.*, high temperature, high oxygen pressure, and specific substrates, are usually needed^{45,46}, which however may oxidize or destroy the bottom layers in the preparing process. In addition, the desired thickness of the spacer layer for IEC investigations is usually less than 5 nm^{8,47}, which calls for high film quality of VO₂ to keep the MIT feature. Therefore, it remains a challenge to insert VO₂ into magnetic layers and guarantee perfect interfaces.

Utilizing the ability of multilayer depositions at ultra-high-vacuum (UHV) with sub-nanometer thickness control accuracy, we choose magnetron sputtering as the deposition method. Through careful adjustment of the target component and systematical study of the deposition condition, ultra-thin VO₂ films have been successfully prepared on different substrates in vacuum at room temperature. **Fig. 1a** shows the XRD results of 2-nm-thick VO₂ film grown on SiO₂/Si substrates. The red lines give the standard XRD pattern of VO₂⁴⁸, while the broad peak indicates an amorphous feature of the film. Further reducing the thickness of VO₂ would make the peak disappear owing to the weakened diffraction intensity, which has also been observed in single crystal samples. XPS measurement was also applied to check the valence states of vanadium. As shown in **Fig. 1b**, the proportion of VO₂ reaches more than 89.3%, which demonstrates the relatively pure composition of the film. To directly check the phase-change feature of the VO₂ film, the resistance of the vertical tunnel junction device fabricated based on Au/VO₂ (2 nm)/Au multilayers is measured at different temperatures. The I-V curves as the temperature rises have been shown in **Fig. 1c**, from which an evolution from tunneling contact to transparent contact can be detected. The results indicate that the resistance of VO₂ spacer layer experiences a significant drop after heating, i.e., MIT happens. **Fig. 1d** gives the resistance change ratio (calculated as the resistance divided by the minimum value) versus temperature with measuring current of 10 nA for the 2 nm sample and a 40 nm single crystal film sample. It's noteworthy that the phase-change of the nanometer VO₂ takes place at a temperature around 310K. Such a value is much lower than that of the thicker one, which can be a result of strain effect. According to some reports, the MIT feature of ultra-thin VO₂ samples is usually suppressed due to impurity diffusions from the substrate⁴⁹. Nevertheless, our room temperature UHV deposition condition may restrain this negative effect. Although potential factors, like the amorphous nature and inevitable defects, still affect the MIT amplitude (~20 times resistance change), the hysteresis phenomenon proves the existence of the phase-change in the ultra-thin film.

The appreciable MIT effect, good-compatibility of the substrates, as well as UHV room temperature deposition condition of the ultra-thin VO₂ film, guarantee the

possibility of fabricating VO₂-related magnetic multilayer systems. To investigate the effect of phase-change modulation on IEC, we prepared a series of [Pt/Co]₂/VO₂/[Co/Pt]₂ heterostructures on SiO₂/Si substrates (see **Fig. 2a** for schematic diagram of the multilayers). VO₂ with different thicknesses are used as the spacer layers and Co/Pt systems are chosen as the perpendicular ferromagnetic layers in these samples. The interface quality has been checked by high resolution transmission electron microscopy (HRTEM), by which the thickness of the spacer layers has also been respectively calibrated as 0.76, 1.48, 1.83 and 2.26 nm (see Supplementary **Fig. S1**). Take the multilayer system with 2.26-nm-thick VO₂ being spacer layer as an example (**Fig. 2b**), distinct interfaces and good continuity between the spacer and the ferromagnetic layers can be observed. Inhomogeneous regions with microcrystalline morphology can also be observed within the VO₂ layer, which may be caused by the fluctuation of sputtering energy and non-annealing process. These inevitable defects also explain the sluggish MIT curve and non-uniform phase change process mentioned in the following discussion. **Fig. 2c** shows the energy dispersive X-ray spectroscopy (EDX) line scan results of elements V, Co, and Pt. Different elements distribution across the multilayered film has been checked, which is consistent with the layer structure. The reason for the overlapping of the two Co peaks that connected to VO₂ layer is caused by the limitation of the electron beam spot (whose size is about 5nm). To further determine the distribution of chemical elements in the multilayer system, EDX mapping of V, Pt and Co are also performed. **Fig. 2d-2f** respectively present the mapping results of different elements, which further verify the good quality of both spacer and ferromagnetic layers.

Fig. 2g gives the schematic diagram of the modulation principle. In the VO₂-related magnetic multilayer system, the magnetic electrons in top and bottom layers are coupled indirectly through VO₂ whose Fermi surface drops on V-3d orbital. As the space layer is insulating at room temperature and conducting at high temperature, according to RKKY theory, the coupling strength or even coupling type would be changed when the density of states near Fermi surface is enhanced. In the following study of this work, we find that the coupling is AFM at room temperature, and evolves

into FM after VO₂ MIT happens. Detailed analysis about the electronic structure change will be discussed later in this article.,

Phase-Change induced IEC regulation

The IEC coupling change of the phase-change magnetic multilayer systems is first investigated by magnetic property measurements. Vibrating sample magnetometer (VSM) and polar magneto-optic Kerr effect (p-MOKE) are used to characterize the [Pt/Co]₂/VO₂/[Co/Pt]₂ samples. As shown in **Fig. 3a**, obvious anisotropy is detected in the sample with 0.76-nm-thick VO₂ spacer layer. Similar PMA property can be found in all the other films (see Supplementary **Fig. S2**). The magnetization shows two reorientation process with out-of-plane magnetic field applied, which indicates that strong ferromagnetic coupling within both top and bottom Co/Pt bilayers. Thus, these bilayers can be assumed as two single ferromagnetic units when the IEC modulation is investigated.

As illustrated in **Fig. 3b-3f**, hysteresis loops are also measured by p-MOKE before (300K, Monoclinic state) and after (360K, Rutile state) phase-change happens for samples with different thicknesses of VO₂. Interestingly, the two magnetization flips merge into one after the MIT happens in the results of 0.76, 1.48, 1.83 and 2.26-nm-thick VO₂ samples. This simultaneous switching phenomenon, implying a strong FM coupling between top and bottom Co/Pt bilayers through the metallic VO₂, gives a solid evidence that the IEC between magnetic layers has been changed. The experimental results of the control samples (with the structure of [Pt/Co]₂/VO₂ and VO₂/[Co/Pt]₂) show that a coercivity difference between the two magnetic layers exists in the whole process, which further exclude the possibility that this phenomenon is merely caused by the modulation on top or bottom magnetic layer (Supplementary **Fig. S3**). In contrast, when the thickness of the spacer layer reaches 3.22 nm (**Fig. 3f**), the two-flip phenomenon maintains even after the phase-change happens, which shows the modulation effect is also restricted by the thickness of the spacer layer. Additionally, the coercivity shrinking values of the two flips are consistent with that of the isolated magnetic layers in the control samples, which indicates a de-coupling state between top and bottom magnetic layers in this sample. These results confirm the possibility of

realizing the modulation of IEC via the MIT of VO₂, while leave more details to be investigated.

To further understand the phase-change induced IEC regulation effect, the first priority is to distinguish the magnetic coupling state at room temperature for the samples that regulation can be observed. Taking the sample with 0.76-nm-thick VO₂ as an example, as the coercive field of the first flip is fairly small (**Fig. 4a**), high-accuracy VSM with built-in Hall probe (accuracy reaches 0.01 Oe) is applied to collect the information of the minor loop. As shown in the inset of Fig. 4a, a negative exchange bias field H_{ex} (~ 0.35 Oe) can be detected in multiple minor loop measurements, which indicates a weak AFM coupling at room temperature. Considering the insulator state of the spacer layer, the small value is reasonable if such a coupling truly exists. To further confirm this result, the magnetic domain switching behavior around the field region of minor loop are also investigated as shown in **Fig. 4b**. The results verify the domain switch fields of the top magnetic layer drop on -0.2 Oe and 1.88 Oe. Meanwhile, similar minor loop measurements are applied to samples with various thicknesses of VO₂ (see Supplementary **Fig. S4**), whose results suggest that the samples with VO₂ of 1.48, 1.83 and 2.26 nm also show weak AFM coupling ($H_{ex}=0.64, 0.30, 0.15$ Oe, respectively) while the sample with 3.22 nm VO₂ shows a decoupling feature ($H_{ex}\approx 0$ Oe).

To obtain more details of the regulation effect, we then focus on the dynamic changing process of IEC effect. **Fig. 4c** shows the hysteresis loops of samples under different temperatures. We find that the flip of the top ferromagnetic layer gradually becomes smoother and eventually coupled with the bottom ferromagnetic layer in all the four samples. Interestingly, the critical IEC type change temperature shows obvious difference in them. For the thinner two samples, the FM coupling change happens above room temperature (around 330 and 325 K), while for the thicker two it happens around 300 K. Considering all the samples are deposited at room temperature with same growth parameters, one possible explanation is that the interfacial strain affects the MIT temperature of VO₂. Similar strain induced transition temperature change has been extensively explored in single crystal VO₂ samples, while happens in thicker region. Considering the inhomogeneous feature of VO₂ in our samples, it is hard to give precise

analysis of the strain effect in the interfacial areas.

To make sure that the IEC modulation is phase change related, the loop evolution process during heating-up and cooling-down is investigated. Considering the phase-change of VO₂ exhibits obvious hysteresis characterization (**Fig. 1d**), it is reasonable to believe a phase-change induced IEC modulation should have the same feature. Therefore, we measured the hysteresis loops of the 0.76-nm-thick VO₂ sample at 305 and 315 K to check the relevance between them. As shown in **Fig. 4d**, the flip sharpness of the results shows clear difference, which proves the hysteresis speculation and further verifies that the coupling change is indeed caused by phase-change of VO₂.

Discussion

Based on the obtained results of [Pt/Co]₂/VO₂/[Co/Pt]₂ multilayer samples, the exchange bias field H_{ex} between two ferromagnetic layers can be derived from the shift of the flip edges referring to control samples.¹⁷ For convenience, we use the flip edge of the bottom layer to calculate the value of H_{ex} . As plotted in **Fig. 5a**, the negative H_{ex} values represent AFM coupling and positive ones represent FM coupling. Samples with various thicknesses of VO₂ all demonstrate a transition from weak AFM coupling at lower temperature (with insulating VO₂) to stronger FM coupling at higher temperature (with metallic VO₂). For each of the four samples, a critical temperature exists, specifying the coupling changing from AFM to FM.

As mentioned above, one possible explanation for the observed coupling change is caused by the electronic structure variation of VO₂ from insulation to metallicity which enhances the coupling between two ferromagnetic layers. To explain the mechanism behind it, the electronic structure and Fermi surface change of spacer layer should be taken into consideration. Abrikosov⁵⁰, as well as Narita and Kasuya^{51,52}, have studied the RKKY interaction mediated by valence conduction band excitations in intrinsic semiconductors in the 1980s. Later Litvinov and Dugaev⁵³ studied the one originated from impurity-valence band excitations in Mn-doped GaAs. As put forward by Goodenough⁵⁴ and elucidated in subsequent studies⁵⁵, d electrons participating in a Peierl-like phase-change exist a large spectral weight transfer from π^* (d_{xy}) into the

valence $d_{//}$ ($d_{xz, yz}$) orbitals. For the MIT of VO_2 induced by temperature change in our experiments, it means that more spin related conducting electrons would participate in the RKKY effect, and contribute to an enhanced coupling effect (**Fig. 5a**). In fact, there were calculation results based on Co-doped TiO_2/VO_2 diluted magnetic semiconductor multilayers reflecting that FM-AFM coupling change may happen accompanied by the phase-change of VO_2 .³³ The reason that coupling oscillation in VO_2 metallic state has not been observed, is probably caused by the restricted range of VO_2 thickness. As our film structure and spin orientation are much more complicated comparing to an ideal model, further calculation and simulations are desired to reveal more detailed physics in it.

Besides the transition from AFM to FM, the loop shape variation in the phase-change process also provides some clue to understand the dynamic spin evolution process. Generally speaking, if the phase-change of VO_2 is uniform across the whole spacer layer, the enhanced coupling would push the magnetization flip away from zero field, before the coupling changes into FM, as illustrated in **Fig. 5b**. While, for the evolution process in our results, the coupling varies accompanied by a smoothing instead of pushing behavior of the first magnetization flip. This phenomenon may be related to the inhomogeneous feature of the ultra-thin VO_2 film mentioned above, and can be explained by a non-uniform phase-change model. The existence of amorphous and microcrystalline VO_2 will result in some conduction boundaries around the inhomogeneous region during the MIT^{56,57}. Thus, the IEC strength increasement is also ununiform in the conducting and insulting areas. The smooth flip is the macroscopic presentation of the non-uniform switching behavior.

To check this speculation, Kerr microscope is then used to observe the domain switching under different temperature. As illustrated in **Fig. 5c**, a magnetic field of 2.6 Oe is applied to the film with 0.76-nm-thick VO_2 to induce a flipping critical state at room temperature. With temperature increase, the magnetic domain first evolves into maze morphology at 310K, then finely broken and becomes more smaller domains which beyond the resolution of the microscope at 315K. With the in-plane loop measurement under different temperature excluding the possibility of anisotropy

change (Supplementary **Fig. S5**), it is reasonable to believe that this domain type change is related to the non-uniform phase change of VO₂ which provides more nucleation points for spin switch. The domain evolution video can be found in Video S1.

In conclusion, we have succeeded in preparing the ultra-thin VO₂ film with appreciable metal-to-insulator transition feature by ultrahigh-vacuum magnetron-sputtering at room temperature. This nanometer-thick VO₂ has been adopted as a spacer layer to regulate the interlayer exchange coupling in a [Pt/Co]₂/VO₂/[Co/Pt]₂ system, whose coupling strength and type can be modulated reversibly and repeatably through the phase-change of VO₂. Further analyses indicate that change of valence band and shift of Fermi surface may answer for the interlayer exchange coupling change. The non-uniform phase-change induced local magnetic domain switching is used to explain the dynamic spin evolution during the transition process. The current result, which combines spintronics with phase-change electronics, offers a new strategy to regulate interlayer exchange coupling, and provides great possibilities for developing new types of electronic devices.

Methods

Film deposition and device fabrication

The Au/VO₂/Au and [Pt/Co]₂/VO₂/[Co/Pt]₂ multilayer systems were both grown on SiO₂/Si substrates by magnetron-sputtering at room temperature under high vacuum environment. Stoichiometric target was used to deposit VO₂ film during the experiments. The tunnel junctions were patterned by optical lithography (Micro Writer ML Baby, Durham Magneto Optics) followed by argon ion-beam etching into bottom electrodes and nanopillars. Then the samples were fully covered with SiO₂ for insulation. After the lift-off procedure, via holes were made over the bottom electrodes. Both the bottom electrodes and tunnel junctions were then connected to 90 nm Ti/Au electrodes to allow electrical contact for measurement using e-beam evaporation.

Characterization and measurement

The magnetic properties were measured by MOKE (NanoMOKE3, Durham Magneto optics ltd) with self-made heat source and VSM (7400, Lakeshore) at different temperatures. The Au/VO₂/Au tunnel junction were measured by normal 4-terminal methods with Keithley 6221 and Keithley 2182 sourcing and measuring units, respectively. The HRTEM was performed by Talos F200X. XPS results were measured by Rigaku D/max-2500PC and XRD measurement was performed by Delta-X.

References

1. Baibich, M. N. *et al.* Giant Magnetoresistance of (001)Fe/(001)Cr Magnetic Superlattices. *Phys. Rev. Lett.* **61**, 2472–2475 (1988).
2. Binasch, G., Grünberg, P., Saurenbach, F. & Zinn, W. Enhanced magnetoresistance in layered magnetic structures with antiferromagnetic interlayer exchange. *Phys. Rev. B* **39**, 4828–4830 (1989).
3. Moodera, J. S., Kinder, L. R., Wong, T. M. & Meservey, R. Large magnetoresistance at room temperature in ferromagnetic thin film tunnel junctions. *Phys. Rev. Lett.* **74**, 3273–3276 (1995).
4. Miyazaki, T. & Tezuka, N. Giant magnetic tunneling effect in Fe/Al₂O₃/Fe junction. *J. Magn. Magn. Mater.* **139**, L231–L234 (1995).
5. Jiang, S., Li, L., Wang, Z., Mak, K. F. & Shan, J. Controlling magnetism in 2D CrI₃ by electrostatic doping. *Nat. Nanotechnol.* **13**, 549–554 (2018).
6. Huang, B. *et al.* Electrical control of 2D magnetism in bilayer CrI₃. *Nat. Nanotechnol.* **13**, (2018).
7. Lin, P. H. *et al.* Manipulating exchange bias by spin–orbit torque. *Nat. Mater.* **18**, 335–342 (2019).
8. Parkin, S. S. P., More, N. & Roche, K. P. Oscillations in exchange coupling and magnetoresistance in metallic superlattice structures: Co/Ru, Co/Cr, and Fe/Cr. *Phys. Rev. Lett.* **64**, 2304–2307 (1990).
9. Parkin, S. S. P., Bhadra, R. & Roche, K. P. Oscillatory magnetic exchange coupling through thin copper layers. *Phys. Rev. Lett.* **66**, 2152–2155 (1991).
10. Parkin, S. S. P. Systematic variation of the strength and oscillation period of indirect magnetic exchange coupling through the 3d , 4d , and 5d transition metals. *Phys. Rev. Lett.* **67**, 3598–3601 (1991).
11. Mosca, D. H. *et al.* Oscillatory interlayer coupling and giant magnetoresistance in Co/Cu multilayers. *J. Magn. Magn. Mater.* **94**, L1–L5 (1991).
12. Toscano, S., Briner, B., Hopster, H. & Landolt, M. Exchange-coupling between ferromagnets through a non-metallic amorphous spacer-layer. *J. Magn. Magn. Mater.* **114**, (1992).

13. Inomata, K., Yusu, K. & Saito, Y. Magnetoresistance Associated with Antiferromagnetic Interlayer Coupling Spaced by a Semiconductor in Fe/Si Multilayers. *Phys. Rev. Lett.* **74**, 1863–1866 (1995).
14. Gareev, R. R. *et al.* Metallic-type oscillatory interlayer exchange coupling across an epitaxial FeSi spacer. *Phys. Rev. Lett.* **87**, 157202/1-157202/4 (2001).
15. Chiba, D., Akiba, N., Matsukura, F., Ohno, Y. & Ohno, H. Magnetoresistance effect and interlayer coupling of (Ga,Mn)As trilayer structures. *Appl. Phys. Lett.* **77**, 1873–1875 (2000).
16. Chung, J. H. *et al.* Carrier-mediated antiferromagnetic interlayer exchange coupling in diluted magnetic semiconductor multilayers $\text{Ga}_{1-x}\text{Mn}_x\text{As}/\text{GaAs:Be}$. *Phys. Rev. Lett.* **101**, 1–4 (2008).
17. Nistor, L. E. *et al.* Oscillatory interlayer exchange coupling in MgO tunnel junctions with perpendicular magnetic anisotropy. *Phys. Rev. B - Condens. Matter Mater. Phys.* **81**, 1–4 (2010).
18. Koziół-Rachwał, A. *et al.* Antiferromagnetic interlayer exchange coupling in epitaxial Fe/MgO/Fe trilayers with MgO barriers as thin as single monolayers. *J. Appl. Phys.* **115**, (2014).
19. Blouzon, C., Ott, F., Torteche, L., Fichou, D. & Moussy, J. B. Anti-ferromagnetic coupling in hybrid magnetic tunnel junctions mediated by monomolecular layers of α -sexithiophene. *Appl. Phys. Lett.* **103**, (2013).
20. Fullerton, E. E., Conover, M. J., Mattson, J. E., Sowers, C. H. & Bader, S. D. 150% magnetoresistance in sputtered Fe/Cr(100) superlattices. *Appl. Phys. Lett.* **63**, 1699–1701 (1993).
21. Ruderman, M. A. & Kittel, C. Indirect Exchange Coupling of Nuclear Magnetic Moments by Conduction Electrons. *Phys. Rev.* **96**, 99–102 (1954).
22. Kasuya, T. A Theory of Metallic Ferro- and Antiferromagnetism on Zener's Model. *Prog. Theor. Phys.* **16**, 45–57 (1956).
23. Yosida, K. Magnetic Properties of Cu-Mn Alloys. *Phys. Rev.* **106**, 893–898 (1957).
24. van Schilfgaarde, M. & Harrison, W. A. Oscillatory exchange coupling: RKKY

- or quantum-well mechanism? *Phys. Rev. Lett.* **71**, 3870–3873 (1993).
25. Bürgler, D. E., Grünberg, P., Demokritov, S. O. & Johnson, M. T. Chapter 1 Interlayer exchange coupling in layered magnetic structures. in *Handbook of Magnetic Materials* **13**, 1–85 (2001).
 26. Qiu, Z. Q. & Smith, N. V. Quantum well states and oscillatory magnetic interlayer coupling. *J. Phys. Condens. Matter* **14**, R169–R193 (2002).
 27. Bruno, P. & Chappert, C. Oscillatory coupling between ferromagnetic layers separated by a nonmagnetic metal spacer. *Phys. Rev. Lett.* **67**, 1602–1605 (1991).
 28. Bruno, P. Theory of interlayer magnetic coupling. *Phys. Rev. B* **52**, 411–439 (1995).
 29. Schäfer, R. Magneto-optical domain studies in coupled magnetic multilayers. *J. Magn. Magn. Mater.* **148**, 226–231 (1995).
 30. Katayama, T. *et al.* Interlayer exchange coupling in Fe/MgO/Fe magnetic tunnel junctions. *Appl. Phys. Lett.* **89**, 12–15 (2006).
 31. Yang, Q. *et al.* Ionic liquid gating control of RKKY interaction in FeCoB/Ru/FeCoB and (Pt/Co)₂/Ru/(Co/Pt)₂ multilayers. *Nat. Commun.* **9**, 1–11 (2018).
 32. Kumar, S. *et al.* Photoinduced antiferromagnetic interlayer coupling in Fe/(Fe-Si) superlattices. *Phys. Rev. Lett.* **71**, 185–188 (1993).
 33. Tang, Z. *et al.* Tuning Interlayer Exchange Coupling of Co-Doped TiO₂/VO₂ Multilayers via Metal-Insulator Transition. *Phys. Rev. Lett.* **107**203, 1–5 (2013).
 34. Liu, P. *et al.* Optically Tunable Magnetoresistance Effect : From Mechanism to Novel Device Application. *Materials (Basel)*. **11**, 47 (2018).
 35. Nakano, M. *et al.* Collective bulk carrier delocalization driven by electrostatic surface charge accumulation. *Nature* **487**, 459–462 (2012).
 36. Lee, S. *et al.* Anomalously low electronic thermal conductivity in metallic vanadium dioxide. *Science* **355**, 371–374 (2017).
 37. Zalba, B, Marin J, Cabeza, L. F. & Mehling, H. *Review on Phase changing materials to store energy*. **23**, (2003).
 38. Farid, M. M., Khudhair, A. M., Razack, S. A. K. & Al-Hallaj, S. A review on

- phase change energy storage: Materials and applications. *Energy Convers. Manag.* **45**, 1597–1615 (2004).
39. Jeyasingh, R., Ahn, E. C., Burc Eryilmaz, S., Fong, S. & Philip Wong, H. S. Phase Change Memory. *Emerg. Nanoelectron. Devices* **9781118447**, 78–109 (2015).
 40. Fan, L. L. *et al.* Growth and phase transition characteristics of pure M-phase VO₂ epitaxial film prepared by oxide molecular beam epitaxy. *Appl. Phys. Lett.* **103**, (2013).
 41. Nagashima, K., Yanagida, T., Tanaka, H. & Kawai, T. Influence of ambient atmosphere on metal-insulator transition of strained vanadium dioxide ultrathin films. *J. Appl. Phys.* **100**, 1–5 (2006).
 42. Yang, T. H., Nori, S., Zhou, H. & Narayan, J. Defect-mediated room temperature ferromagnetism in vanadium dioxide thin films. *Appl. Phys. Lett.* **95**, 1–4 (2009).
 43. Gupta, A., Narayan, J. & Dutta, T. Near bulk semiconductor to metal transition in epitaxial VO₂ thin films. *Appl. Phys. Lett.* **97**, 1–4 (2010).
 44. Vernardou, D., Pemble, M. E. & Sheel, D. W. Vanadium oxides prepared by liquid injection MOCVD using vanadyl acetylacetonate. *Surf. Coatings Technol.* **188–189**, 250–254 (2004).
 45. Wang, Y. *et al.* Defect-engineered epitaxial VO_{2±δ} in strain engineering of heterogeneous soft crystals. *Sci. Adv.* **4**, 1–11 (2018).
 46. Lee, D. *et al.* Isostructural metal-insulator transition in VO₂. *Science* **362**, 1037–1040 (2018).
 47. Li, X. X., Bao, J., Lu, L. Y., Xu, X. G. & Jiang, Y. Oscillatory antiferromagnetic interlayer coupling in Co/Pt multilayer with perpendicular anisotropy. *Solid State Commun.* **148**, 209–212 (2008).
 48. Rogers, K. D. An X-ray diffraction study of semiconductor and metallic vanadium dioxide. *Powder Diffr.* **8**, 240–244 (1993).
 49. Zhi, B. *et al.* Thickness-dependent metal-to-insulator transition in epitaxial VO₂ films. *Mater. Res. Express* **1**, 046402 (2014).

50. Abrikosov, A. A. Spin-glass with a semiconductor as host. *J. Low Temp. Phys.* **39**, 217–229 (1980).
51. Narita, A. & Kasuya, T. Magnetic exchange interactions and spin structures in some rare earth pnictides. *J. Magn. Magn. Mater.* **52**, 373–376 (1985).
52. Narita, A. Analytic structures of rky interactions in magnetic semiconductors and in materials with a gap on the fermi surface. *J. Phys. C Solid State Phys.* **19**, 4797–4808 (1986).
53. Litvinov, V. I. & Dugaev, V. K. Ferromagnetism in magnetically doped III-V semiconductors. *Phys. Rev. Lett.* **86**, 5593–5596 (2001).
54. Goodenough, J. B. The two components of the crystallographic transition in VO₂. *J. Solid State Chem.* **3**, 490–500 (1971).
55. Eyert, V. The metal-insulator transitions of VO₂: A band theoretical approach. *Ann. der Phys.* **11**, 650–702 (2002).
56. Kawatani, K., Takami, H., Kanki, T. & Tanaka, H. Metal-insulator transition with multiple micro-scaled avalanches in VO₂ thin film on TiO₂ (001) substrates. *Appl. Phys. Lett.* **100**, 173112 (2012).
57. Kanki, T., Kawatani, K., Takami, H. & Tanaka, H. Direct observation of giant metallic domain evolution driven by electric bias in VO₂ thin films on TiO₂ (001) substrate. *Appl. Phys. Lett.* **101**, 243118 (2012).

Figures & Legends:

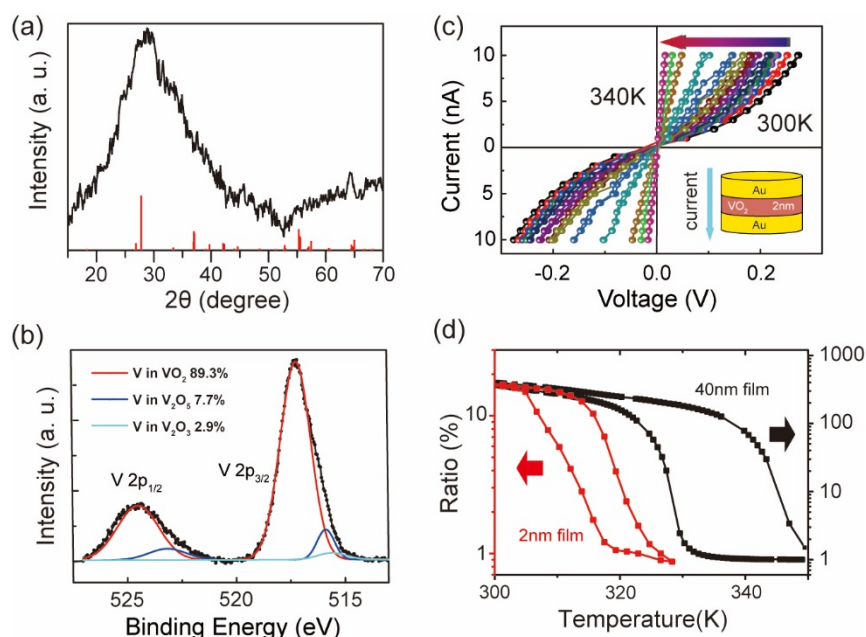


Figure 1 | Characterization of 2-nm-thick VO₂ film grown by sputtering. (a) XRD θ - 2θ scan of 2-nm-thick VO₂ prepared on SiO₂/Si substrates. The red lines give the standard XRD pattern of VO₂. (b) XPS profile of the sample with peak fitting results. The proportion of VO₂ reaches more than 89.3% (c) I-V curve of the VO₂ tunnel junction measured at different temperatures with the current flows vertically through the device. The insert gives the schematic of the tunnel junction which is fabricated based on Au/VO₂ (2 nm)/Au multilayer. (d) The resistance change ratio versus temperature of 2 nm and 40 nm VO₂ films which indicates the existence of MIT feature.

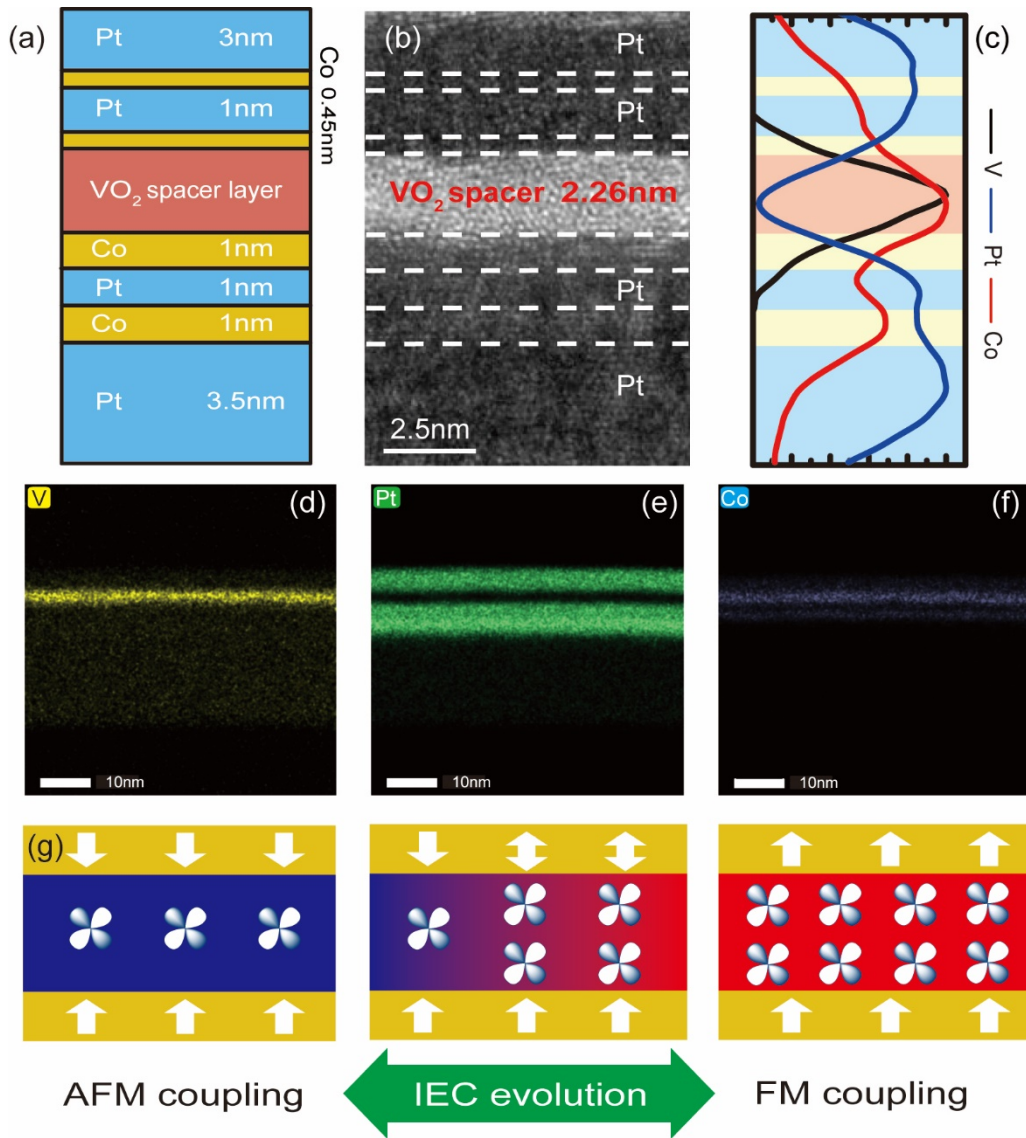


Figure 2 | Interface characterization of [Pt/Co]₂/VO₂/[Co/Pt]₂ multilayer system performed by HRTEM. (a) The schematic of the multilayer system. (b) HRTEM image of the 2.26 nm VO₂ spacer sample that shows distinct interfaces with good continuity between the spacer and the ferromagnetic layers. (c) The line scanning results of V, Co and Pt elements. (d)-(f) EDX mappings of V, Pt and Co, respectively. (g) Schematic diagram of the interlayer exchange coupling (IEC) modulation principle

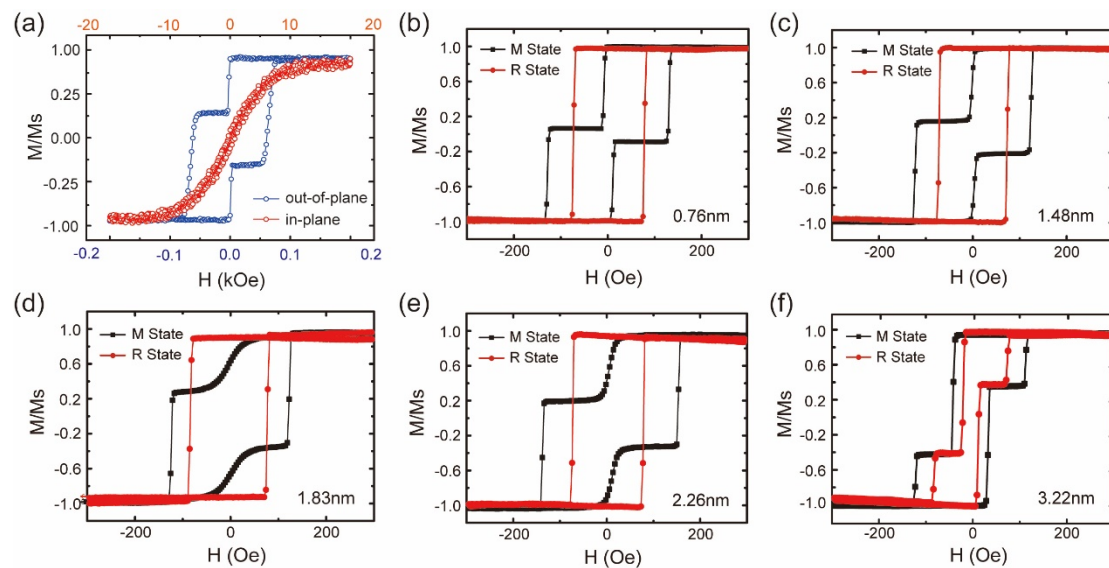


Figure 3 | The magnetic properties of [Pt/Co]₂/VO₂/[Co/Pt]₂ multilayer measured by VSM and p-MOKE. (a) Hysteresis loops of [Pt/Co]₂/VO₂/[Co/Pt]₂ multilayer measured by VSM with magnetic field applied in-plane field (red line) and out-of-plane field (blue line) which shows the PMA feature of the multilayer system. **(b)-(f)** Hysteresis loops of the multilayer systems before (300K) and after (360K) phase-change measured by p-MOKE, where the thickness of VO₂ is 0.76, 1.48, 1.83, 2.26 and 3.22 nm, respectively. M state and R state in the figures stand for monoclinic and rutile structure state, respectively.

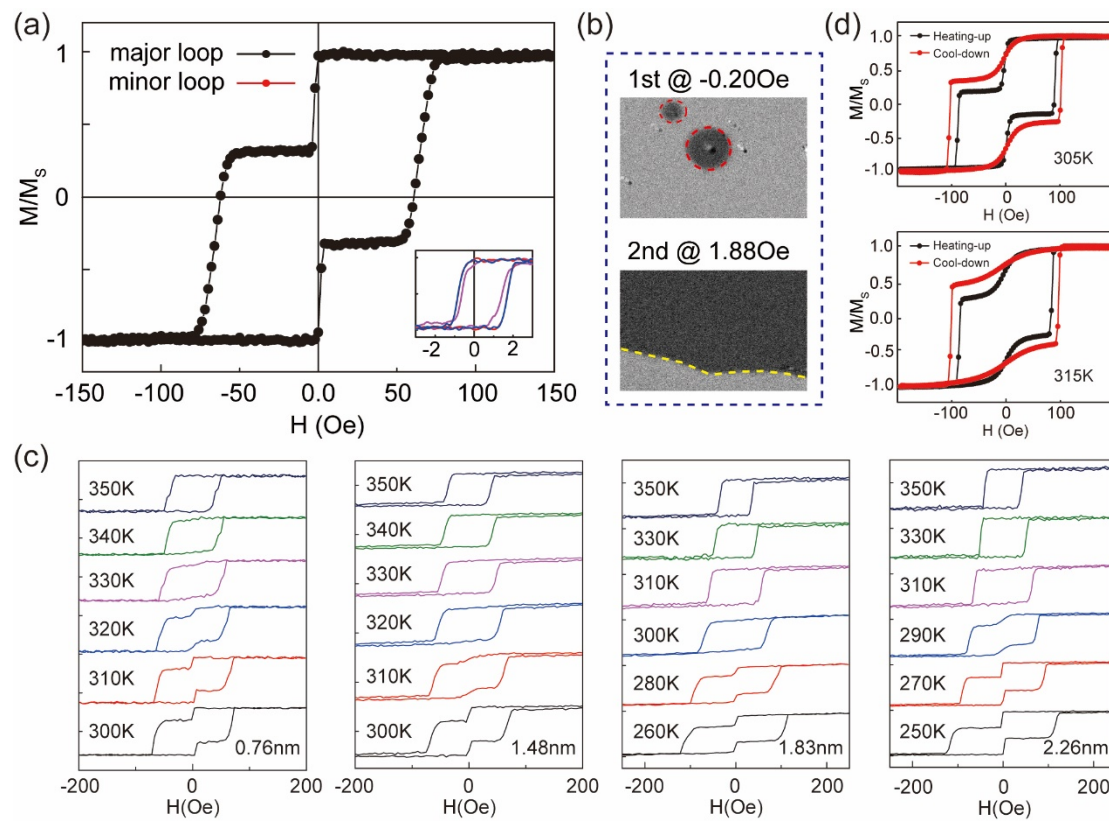


Figure 4 | The regulation of IEC in the multilayers during phase-change process.

(a) The major and minor loops of the multilayer system with 0.76-nm-thick VO₂ measured by VSM. (b) The magnetic domain switching behaviour around the minor loop field region observed by Kerr microscope. (c) The variation of hysteresis loops as temperature rising for samples with VO₂ of 0.76, 1.48, 1.83, 2.26nm respectively. (d) The comparison of the hysteresis loops between heating-up and cool-down process at 305 K and 315 K.

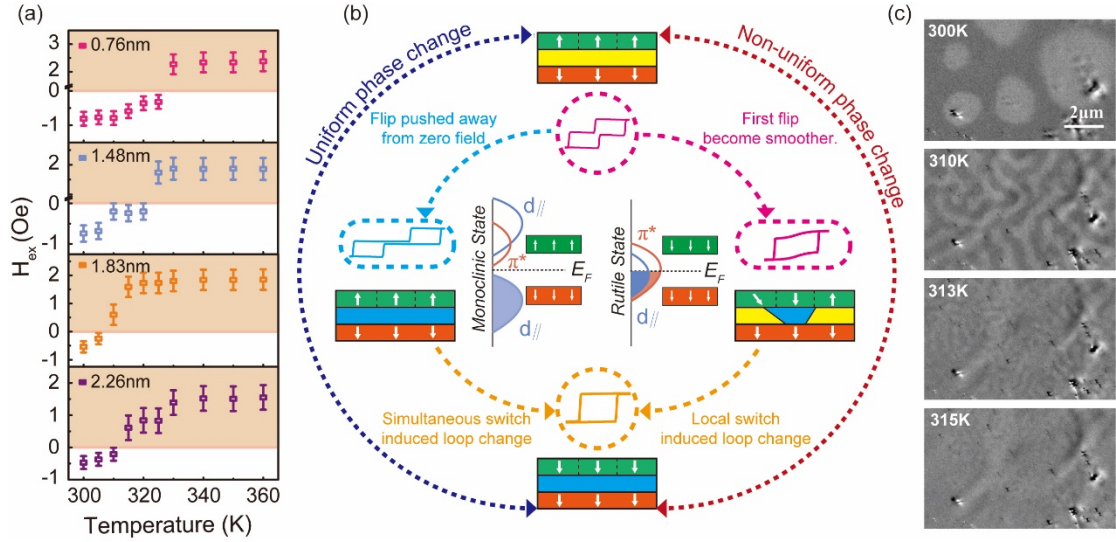


Figure 5 | Physical mechanism of IEC regulation via phase-change. (a) Exchange coupling field versus temperature for VO_2 thicknesses of 0.76, 1.48, 1.83 and 2.26 nm, respectively. (b) Change of valence band and Fermi surface during phase-change, as well as the different dynamic spin evolution process. (c) The magnetic domain morphology of 0.76-nm-thick VO_2 film observed by Kerr microscope under different temperature with the field of 2.6Oe applied.

Supplementary Materials

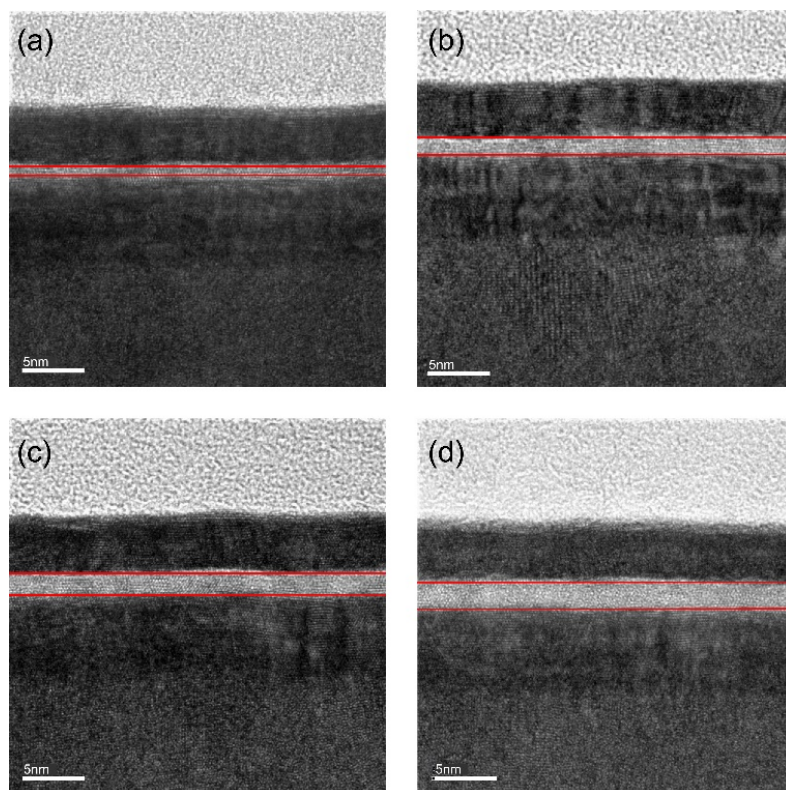


Figure S1 | Interface characterization of $[\text{Pt/Co}]_2/\text{VO}_2/[\text{Co/Pt}]_2$ multilayer systems performed by HRTEM. Thickness of VO_2 calibrated to be 0.76 (a), 1.48 (b), 1.83 (c) and 2.26 (d) nm.

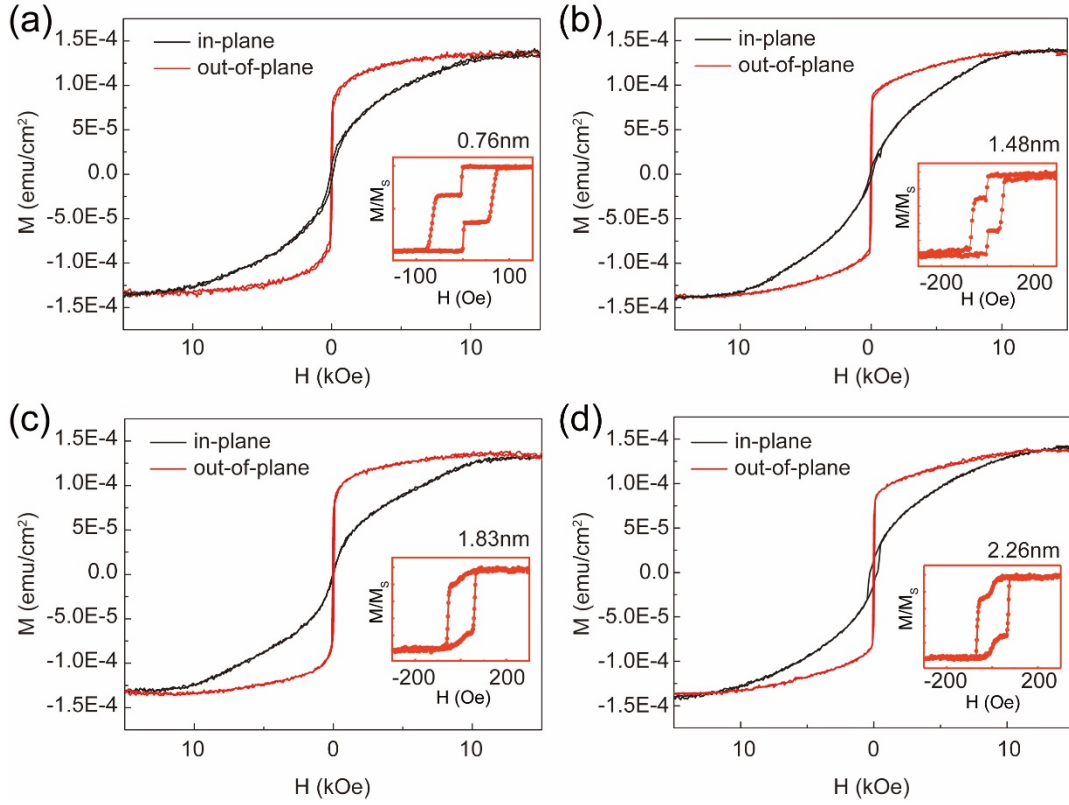


Figure S2 | The magnetic properties of $[\text{Pt/Co}]_2/\text{VO}_2/[\text{Co/Pt}]_2$ multilayer systems. (a)-(d) represent the thickness of VO_2 is 0.76, 1.48, 1.83, 2.26nm respectively. The inset gives the enlarged result out of plane.

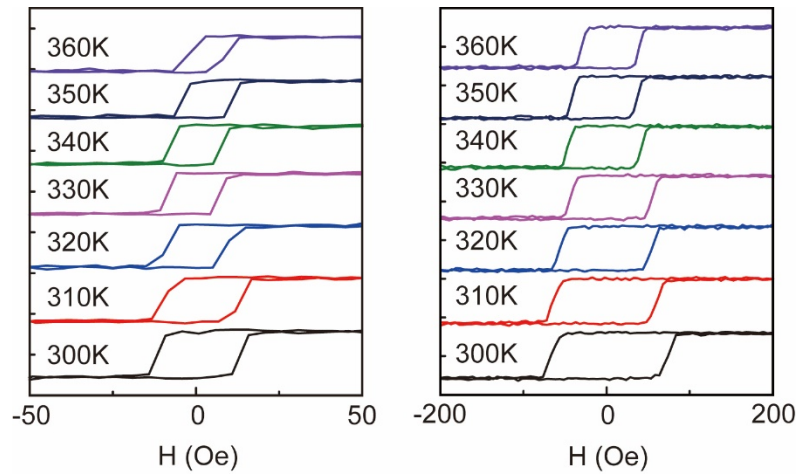


Figure S3 | The magnetic properties of the reference samples. (a) and (b) represent the single top ferromagnetic layer with VO_2 ($[\text{Pt/Co}]_2/\text{VO}_2$) and bottom layer ($\text{VO}_2/[\text{Co/Pt}]_2$) with temperature rising from 300K to 335K measured by p-MOKE.

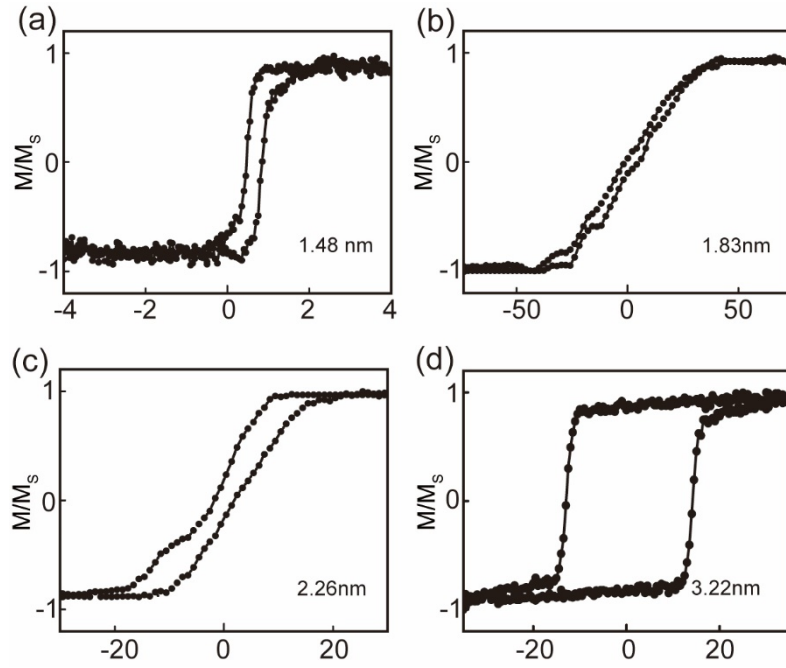


Figure S4 | The minor loops of $[\text{Pt/Co}]_2/\text{VO}_2/[\text{Co/Pt}]_2$ multilayer systems measured by VSM at room temperatures. (a)-(d) represent the thickness of VO_2 is 1.48, 1.83, 2.26 and 3.22 nm. The exchange field is 0.64, 0.30, 0.15 and 0 Oe, respectively.

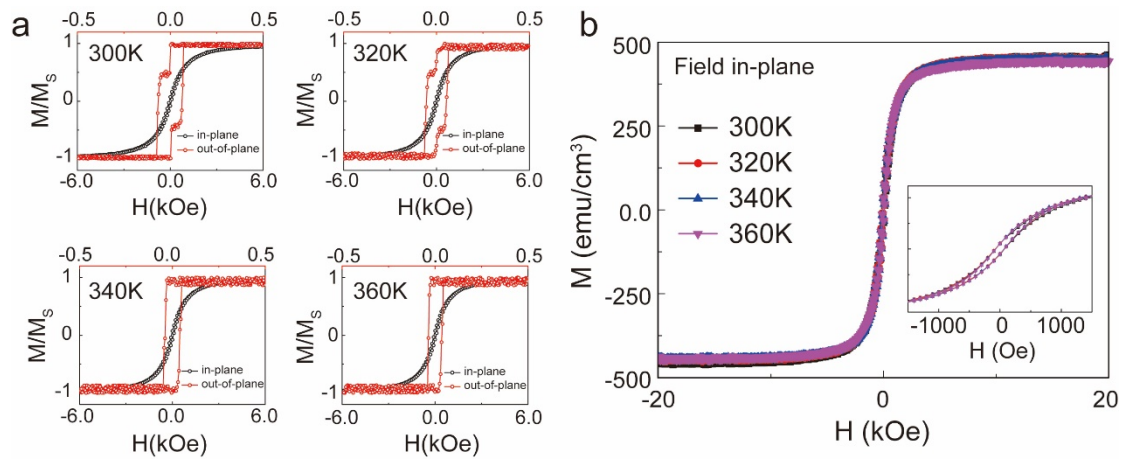


Figure S5 | Hysteresis loop measurements for the 0.76-nm-thick VO_2 sample. (a) Hysteresis loops of the sample at different temperatures with field applied in-plane and out-of-plane. **(b)** In-plane loop results under different temperature, which shows no indication of anisotropy change.